Kinetic and Thermodynamic Studies of Silica Nanoparticle Dissolution

Jeffrey D. Rimer,[†] Olga Trofymluk,[‡] Alexandra Navrotsky,[‡] Raul F. Lobo,*[,†] and Dionisios G. Vlachos*[,†]

Center for Catalytic Science and Technology, Department of Chemical Engineering, University of Delaware, Newark, Delaware 19716, and Thermochemistry Facility and NEAT ORU, University of California at Davis, Davis, California 95616

Received March 14, 2007. Revised Manuscript Received May 23, 2007

Small-angle X-ray scattering (SAXS) and microcalorimetry were used to study the dissolution of silica nanoparticles that serve as precursors in the synthesis of the pure-silica zeolite, silicalite-1. Temporal changes in nanoparticle size were monitored by SAXS to obtain radial dissolution rates on the order of 1×10^{-2} nm/min, 10 times greater than those of silicalite-1. Nanoparticle dissolution rates are independent of solution alkalinity (above pH 11) and particle surface area, although contributions from the latter account for more than 60% of the nanoparticle enthalpy of dissolution (13.5 ± 0.1 kJ/mol SiO_2 relative to silicalite-1). We show that dissolution enthalpies and rates correlate to the molecular structure of silicates. Comparisons among amorphous silica, silicalite-1, and silica nanoparticles suggest that the latter are amorphous and therefore not simply small fragments of a crystalline zeolite. Nevertheless, they do possess a degree of ordering greater than that in dense amorphous silica. Dissolution experiments were also performed on heat-treated nanoparticles grown via Ostwald ripening. With increasing time of heat treatment, the nanoparticle dissolution rates and enthalpies decrease in magnitude toward those of silicalite-1, suggesting a structural reorganization of silica within the particles. The results offer insight on silicalite-1 nucleation as well as relevant time scales and rate-determining steps involved in zeolite crystallization.

1. Introduction

Identifying the role of silica nanoparticles in zeolite nucleation and growth is important for quantifying and controlling the properties of these materials for implementation in optical or electronic devices,[1] selective separations,[2−7] and other applications.[8,9] The synthesis of silicalite-1 (MFI framework type) has served as a prototype for mechanistic studies of zeolite crystallization (see Figure 1b). In this paper, we investigate the nanoparticles formed in precursor solutions of silicalite-1, synthesized using the structure-directing agent tetrapropylammonium (TPA^+).

Silica nanoparticles (1−6 nm) are formed in solutions of tetraethylorthosilicate, water, and a strong base, M^+OH^-, through spontaneous self-assembly above a specific silica concentration (i.e., SiO_2 solubility).[10,11] Nanoparticles serve as precursors in clear solution syntheses of microporous[12−15] and mesoporous[16,17] silica materials. The nanoparticles are comprised of covalently bound silica with silanol groups that dissociate above pH 10, thus giving the particles a negative charge. Counterions, M^+, are typically small organocations[18] or alkali metal cations that associate with the nanoparticle surface via electrostatic and/or hydrophobic forces. Counterions in microporous syntheses are typically small organic cations that act as structure-directing agents (SDAs) in zeolite crystallization. The relatively low hydrophobicity of SDAs[18−21] inhibits cation self-association at typical concentrations and

* Corresponding author. Phone: 302-831-1261 (R.F.L.); 302-831-2830 (D.G.V.). E-mail: lobo@udel.edu (R.F.L.); vlachos@udel.edu (D.G.V.).
† University of Delaware.
‡ University of California at Davis.

(1) Tosheva, L.; Valtchev, V. P. *Chem. Mater.* **2005**, *17*, 2494.
(2) Lai, Z.; Bonilla, G.; Diaz, I.; Nery, J. G.; Sujaoti, K.; Amat, M. A.; Kokkoli, E.; Terasaki, O.; Thompson, R. W.; Tsapatsis, M.; Vlachos, D. G. *Science* **2003**, *300*, 456.
(3) Lai, Z. P.; Tsapatsis, M.; Nicolich, J. R. *Adv. Funct. Mater.* **2004**, *14*, 716.
(4) Lee, J. S.; Lee, Y. J.; Tae, E. L.; Park, Y. S.; Yoon, K. B. *Science* **2003**, *301*, 818.
(5) Miyamoto, M.; Kamei, T.; Nishiyama, N.; Egashira, Y.; Ueyama, K. *Adv. Mater.* **2005**, *17*, 1985.
(6) Walker, A. M.; Slater, B.; Gale, J. D.; Wright, K. *Nat. Mater.* **2004**, *3*, 715.
(7) Kirschhock, C. E. A.; Kremer, S. P. B.; Vermant, J.; Van Tendeloo, G.; Jacobs, P. A.; Martens, J. A. *Chem.—Eur. J.* **2005**, *11*, 4306.
(8) Wan, Y. S. S.; Chau, J. L. H.; Gavriilidis, A.; Yeung, K. L. *Microporous Mesoporous Mater.* **2001**, *42*, 157.
(9) Zampieri, A.; Colombo, P.; Mabande, G. T. P.; Selvam, T.; Schwieger, W.; Scheffler, F. *Adv. Mater.* **2004**, *16*, 819.
(10) Fedeyko, J. M.; Rimer, J. D.; Lobo, R. F.; Vlachos, D. G. *J. Phys. Chem. B* **2004**, *108*, 12271.
(11) Fedeyko, J. M.; Vlachos, D. G.; Lobo, R. F. *Langmuir* **2005**, *21*, 5197.
(12) Cundy, C. S.; Cox, P. A. *Microporous Mesoporous Mater.* **2005**, *82*, 1.
(13) Auerbach, S. M.; Carrado, K. A.; Dutta, P. K. *Handbook of Zeolite Science and Technology*; Marcel Dekker: New York, 2003.
(14) Wakihara, T.; Okubo, T. *Chem. Lett.* **2005**, *34*, 276.
(15) Knight, C. T. G.; Wang, J. P.; Kinrade, S. D. *Phys. Chem. Chem. Phys.* **2006**, *8*, 3099.
(16) Rimer, J. D.; Fedeyko, J. M.; Vlachos, D. G.; Lobo, R. F. *Chem.—Eur. J.* **2006**, *12*, 2926.
(17) Fedeyko, J. M.; Vlachos, D. G.; Lobo, R. F. *Microporous Mesoporous Mater.* **2006**, *90*, 102.
(18) Lobo, R. F.; Zones, S. I.; Davis, M. E. *J. Inclusion Phenom. Mol. Recogn. Chem.* **1995**, *21*, 47.
(19) Burton, A. W.; Zones, S. I.; Elomari, S. *Curr. Opin. Colloid Interface Sci.* **2005**, *10*, 211.
(20) Burton, A. W.; Lee, G. S.; Zones, S. I. *Microporous Mesoporous Mater.* **2006**, *90*, 129.
(21) Goretsky, A. V.; Beck, L. W.; Zones, S. I.; Davis, M. E. *Microporous Mesoporous Mater.* **1999**, *28*, 387.

10.1021/cm070708d CCC: $37.00
Published on Web 07/26/2007

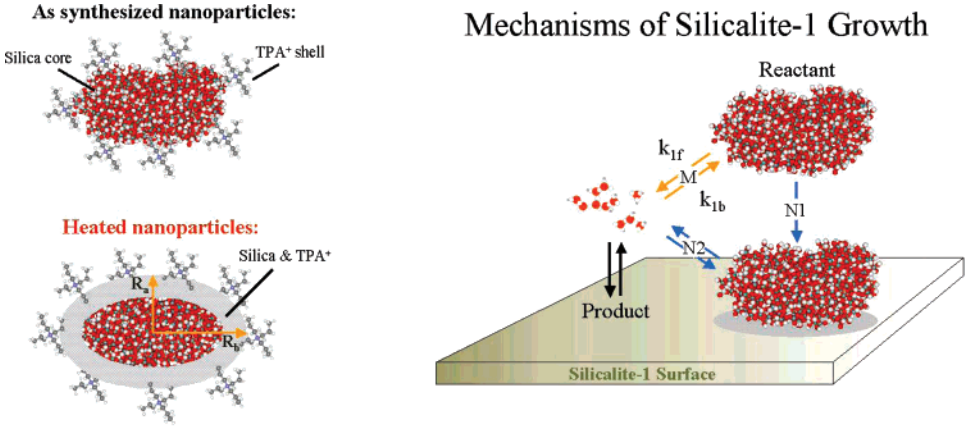

Figure 1. (a) Schematic representation of as-synthesized (top) and heated (bottom) silica nanoparticles. The former have a core−shell structure consisting of a SiO_2 core surrounded by an adsorbed cation shell (labeled as TPA^+ for silicalite-1 precursor solutions). Heated nanoparticles (grown by Ostwald ripening) have a core comprised of TPA^+ and SiO_2, the thickness, exact composition, and structure of which are unknown. Particle morphology has been identified as either polydisperse spheres or oblate ellipsoids and is presented here as the latter with radial axes R_a and R_b. (b) Schematic diagram of silicalite-1 growth illustrating three proposed mechanisms in the literature: (1) "monomer addition" involving the dissolution of nanoparticles, path *M*, to monomers/oligomers that add to the zeolite surface;[55] (2) "nanoparticle addition" whereby nanoparticles (disordered or partially crystalline) adsorb to the surface (path *N1*) and undergo rearrangement (path *N2*) to form the crystalline product;[35] and (3) direct addition (path *N1*) of crystalline nanoparticles with little to no rearrangement.[7,51]

leads to charge-stabilized,[22] core−shell[11] nanoparticles consisting of a hydrated silica core surrounded by a layer of adsorbed cations (see Figure 1a).

Silica−TPA^+ nanoparticles are thermodynamically metastable.[23] Heating during the early stages of nucleation results in an Ostwald ripening process (see Figure 1a), where some nanoparticles grow at the expense of others that dissolve.[24] Growth is accompanied by a shift in nanoparticle composition toward that of silicalite-1.[24] However, it is not known how the molecular structure and arrangement of silica (and TPA^+) within the nanoparticle core changes during this heating process. The structure of nanoparticles (in particular whether particles are more like amorphous silica or more like a crystalline zeolite) has been the subject of intense debate, given that attempts to probe their long-range order have been inconclusive.[15,25] For example, X-ray diffraction (XRD) cannot be used to provide evidence for or against crystallinity at the nanoscale, because the particle size is too small to generate Bragg peaks in the scattering patterns. Techniques such as Fourier transform infrared spectroscopy (FTIR) and ^{29}Si NMR mainly provide information on nearest neighbor connectivities, but not mid- or long-range order. Although some data in the literature suggest silica nanoparticles are similar to amorphous silica,[25] no direct evidence of their molecular structure has been obtained.

In this paper, we use small-angle X-ray scattering (SAXS) and microcalorimetry to investigate TPA−silica nanoparticles. SAXS was used previously to study silicalite-1 precursor solutions, yielding information on nanoparticle size,[10,26] morphology,[11,27] and composition.[24] Microcalorimetry has been used to investigate various aspects of silicalite-1 crystallization.[28−31] Here, we combine both techniques to analyze the dissolution of silica nanoparticles. Dissolution experiments are performed on as-synthesized and heat-treated nanoparticles to observe their structural evolution. The combined results from these studies are put into a broader perspective of nanoparticle structure and silicalite-1 crystallization.

2. Experimental Methods

2.1. Synthesis and Dissolution Studies. Silica nanoparticles were synthesized by mixing tetrapropylammonium hydroxide (TPAOH, Alfa Aesar, 40 w/%) with deionized water, followed by the addition of tetraethylorthosilicate (TEOS, Aldrich, 98%) to obtain an *X*:*Y*:9500:4*Y* TPAOH:SiO_2:H_2O:EtOH molar composition. Solutions of varying alkalinity ($X = 4.5$, 9, 18, and 27) and silica concentration ($Y = 40$, 60, and 80) were prepared to study the effects of nanoparticle size and number density. Nanoparticle solutions were continuously stirred for 12 h and filtered with a 0.45 μm membrane (Pall Corp.) prior to analysis. We denote these "as-synthesized" nanoparticles (i.e., prepared at room temperature), and they serve as the reference point for comparing particles grown at higher temperatures. All nanoparticle solutions contain the ethanol formed during the hydrolysis of TEOS. Thermal treatment was performed by placing 10 mL of solution in sealed polypropylene tubes that were submerged in a water bath regulated to ±0.1 °C at chosen temperatures in the range 25−70 °C. Equilibrium temperature was reached within 5 min of heating, and the individual samples were removed at various times and quenched in an ice bath.

Dissolution of silica nanoparticles was induced by increasing pH through the addition of TPAOH to the solutions while stirring at room temperature. Samples were immediately placed in polypropylene tubes, heated in the water bath, and removed at various times and stored in ice to stop any further dissolution. Two alkalinities were studied with total TPAOH concentrations of 0.3 and 0.5 M.

(22) Rimer, J. D.; Lobo, R. F.; Vlachos, D. G. *Langmuir* **2005**, *21*, 8960.
(23) Jorge, M.; Auerbach, S. M.; Monson, P. A. *J. Am. Chem. Soc.* **2005**, *127*, 14388.
(24) Rimer, J. D.; Vlachos, D. G.; Lobo, R. F. *J. Phys. Chem. B* **2005**, *109*, 12762.
(25) Kragten, D. D.; Fedeyko, J. M.; Sawant, K. R.; Rimer, J. D.; Vlachos, D. G.; Lobo, R. F.; Tsapatsis, M. *J. Phys. Chem. B* **2003**, *107*, 10006.
(26) de Moor, P.; Beelen, T. P. M.; van Santen, R. A. *J. Phys. Chem. B* **1999**, *103*, 1639.
(27) Watson, J. N.; Iton, L. E.; Keir, R. I.; Thomas, J. C.; Dowling, T. L.; White, J. W. *J. Phys. Chem. B* **1997**, *101*, 10094.
(28) Yang, S. Y.; Navrotsky, A. *Chem. Mater.* **2002**, *14*, 2803.
(29) Yang, S. Y.; Navrotsky, A. *Chem. Mater.* **2004**, *16*, 3682.
(30) Yang, S. Y.; Navrotsky, A.; Wesolowski, D. J.; Pople, J. A. *Chem. Mater.* **2004**, *16*, 210.
(31) Navrotsky, A. *Curr. Opin. Colloid Interface Sci.* **2005**, *10*, 195.

Table 1. Molar Compositions and Concentrations for Nanoparticle Syntheses and Dissolution

	synthesis composition and pH[a]			dissolution concn (M)[b]	
sample	Y SiO_2	X TPAOH	pH	$[SiO_2]_{tot}$	[TPAOH]
S1	80	27.0	11.5	0.4	0.5
S2	40	9.0	11.0	0.2	0.3
S3	60	9.0	10.8	0.3	0.3
S4	40	4.5	10.4	0.2	0.3
S5	80	9.0	10.6	0.4	0.3
S6	80	9.0	10.6	0.4	0.5

[a] Molar compositions, Y:X:9500:4Y SiO_2:TPAOH:H_2O:EtOH, of as-synthesized particles. [b] $[SiO_2]_{tot}$ and [TPAOH] values correspond to the concentrations after TPAOH addition to as-synthesized nanoparticle solutions.

Table 1 lists the compositions of solutions, labeled as samples S1−S6, and their concentrations following TPAOH addition.

Silicalite-1 crystals (diameter ≈ 130 nm) were synthesized following the protocol of Hedlund et al.,[32] in which TPAOH was mixed with deionized water, followed by the addition of TEOS to obtain a 9:25:1450:100 TPAOH:SiO_2:H_2O:EtOH molar composition. The solution was stirred overnight at room temperature and placed into a sealed, Teflon-lined autoclave that was heated in an oven at 100 °C for 48 h. Silicalite-1 crystals were washed with deionized water, separated by ultracentrifugation (13,000 rpm), and decanted to remove the excess ethanol, soluble silica, and TPAOH. The wash/centrifugation procedure was performed a total of three times, and the isolated particles were stored in deionized water (stock solution contains ∼0.1 g of particles per 1.0 g of H_2O).

Dissolution studies of silicalite-1 particles were conducted by placing ∼1.0 g of stock solution in 110 g of aqueous solutions of TPAOH. TPAOH and water were mixed to give a desired pH and filtered with a 0.45 μm membrane, followed by particle addition and sonification. Samples were placed in sealed, 15 mL polypropylene tubes and submerged in a water bath regulated at 70−95 °C. Samples were removed at various times, allowing ∼10 min prior to the first removal, and were kept in an ice bath before measurement.

Amorphous silica Stöber[33] particles were synthesized following the protocol reported by Bogush et al.[34] In one container was placed 15.00 g of ethanol (Sigma-Aldrich, 99.5%), 1.42 g of ammonium hydroxide (Aldrich, 28−30% NH_3), and 9.00 g of deionized water. In a separate container, 23.00 g of ethanol and 2.08 g of TEOS were mixed, and the contents of both containers were then combined. The resulting mixture was stirred at room temperature for 6 h, after which the particles (diameter ≈ 250 nm) were isolated by several ethanol wash and centrifuge cycles. The particles were stored in ethanol (0.06 g of silica per 1.0 g of ethanol) and a fraction was dried for calorimetry measurements. Dissolution studies were performed by first placing ∼1.0 g of stock solution in 0.3 M TPAOH (previously filtered), sonifying the mixture to break potential aggregates, and heating the sample according the procedure for silicalite-1.

2.2. Particle Size Measurements. Nanoparticle size was measured by SAXS using a SAXSess (Anton-Paar) instrument. Samples were placed in a vacuum-tight 1 mm diameter quartz capillary holder, and measured at 15 °C (allowing ∼8 min for temperature equilibration). A monochromatic, line-collimation source of CuK_α radiation ($\lambda = 1.54$ Å) was used with a 265 mm sample-to-detector distance. The scattering patterns were collected over a 30 min period within the q-range 0.1−8 nm^{-1}. Patterns were normalized to the height of the primary beam signal, and the background (i.e., deionized water) signal was subtracted for each sample.

Sizing of silicalite-1 and Stöber particles were conducted by dynamic light scattering (DLS) using a Brookhaven Instruments BI9000AT correlator and BI200SM goniometer. Samples were placed in a decalin index-matching bath and illuminated with a 488 nm laser source (Lexel 95 2 W argon laser). All measurements were performed at a scattering angle of 90° and a temperature of 25 °C. The intensity autocorrelation function was analyzed by the method of cumulants (quadratic). Four measurements (1 min each) were taken to allow statistical averaging. The diameters were corrected for solution viscosity, which was obtained with a Cannon−Ubbelohde capillary viscometer and a Cannon CT-1000 constant temperature bath. Deionized water (0.89 cP at 25 °C) was used to calibrate the viscometer. Solutions at pH 12.9 and 13.5 resulted in viscosities of 0.96 and 1.21 cP, respectively. Viscosities of solutions at lower pH were equal within experimental error to that of pure water.

2.3. Calorimetry. A Setaram C-80 Calvet twin microcalorimeter was used to obtain enthalpies of dissolution. The calorimeter was operated isothermally at 28.00 ± 0.01 °C. Samples (1.0 g) were placed in a Teflon-lined stainless steel reaction cell, and the same amount of deionized water was placed in a reference cell. After the nanoparticle solution was allowed to equilibrate at the desired temperature and the calorimeter reached a steady baseline, 0.12 g of TPAOH was contacted with the nanoparticle solution by the downward push of a retractable rod. This rod dropped a small plug into the cell, exposing the TPAOH to the nanoparticle mixture. Although it was not possible to stir the reaction mixture, the completion of the dissolution reaction was easily identified by the return of the heat flow signal to a stable constant value. An empty plug was simultaneously released in the reference cell to correct for any mechanical disturbance. The reaction enthalpy was obtained from the heat flow data by integrating the peaks over time, and converting the peak area to enthalpy by a calibration factor, obtained by electrical calibration. The heat of TPAOH dilution was measured similarly to that of nanoparticle dissolution, using a mixture of 9:9500:160 TPAOH:H_2O:EtOH molar composition in the reaction cell.

Microcalorimetry of Stöber particles was performed following the same protocol. A 0.23 M TPAOH/H_2O mixture (1.0 g) was placed in Teflon-lined stainless steel reaction and reference cells. After the setup was allowed to equilibrate and the calorimeter reached a steady baseline, 10 mg of amorphous silica (dry powder) was contacted with TPAOH by the downward push of a retractable rod. The heats of reaction for silicalite-1 dissolution were obtained by first placing 7.0 g of silicalite-1 (12 mg SiO_2 in 0.23 M TPAOH) in a sealed Teflon-lined stainless steel vessel. A heat flow signal was recorded using deionized water as a reference to reduce baseline offset. The temperature was increased from 22 to 110 °C at 0.1 °C/min.

2.4. Conductivity and pH. All silicate samples stored in ice were allowed ∼15 min to reach room temperature prior to pH and conductivity measurements. The ionic conductivity (±0.02 mS/cm) was obtained with a VWR model 2052 EC meter and the pH (±0.05) was measured using a Corning 355 pH/ion analyzer and a WTW SenTix 61 pH combination electrode. The pH meter was calibrated with standardized pH 7, 10, and 12 buffer solutions (Alfa Aesar).

3. Results and Calculations

3.1. Silica Nanoparticle Dissolution. *3.1.1. Nanoparticles and the Aqueous Silica Phase Diagram in TPAOH Solutions.*

(32) Hedlund, J.; Mintova, S.; Sterte, J. *Microporous Mesoporous Mater.* **1999**, *28*, 185.
(33) Stober, W.; Fink, A.; Bohn, E. *J. Colloid Interface Sci.* **1968**, *26*, 62.
(34) Bogush, G. H.; Tracy, M. A.; Zukoski, C. F. *J. Non-Cryst. Solids* **1988**, *104*, *95*.

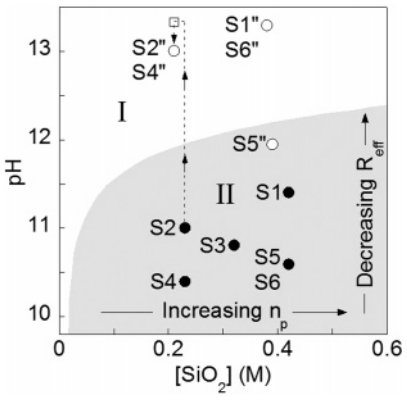

Figure 2. Aqueous silica phase diagram of pH vs total silica concentration, with region I containing soluble silica in the form of monomers and oligomers and region II (shaded) containing nanoparticles in equilibrium with soluble silica. Solid symbols represent the compositions of as-synthesized nanoparticle solutions prior to TPAOH addition. Nanoparticle number density, n_p, increases from left to right and the particle radius decreases from bottom to top. Open symbols are equilibrium solutions after dissolution is complete. Dashed lines with arrows illustrate the changes in S2 solutions from the addition of TPAOH to completion, where the open square symbol marks the pH at the onset of dissolution.

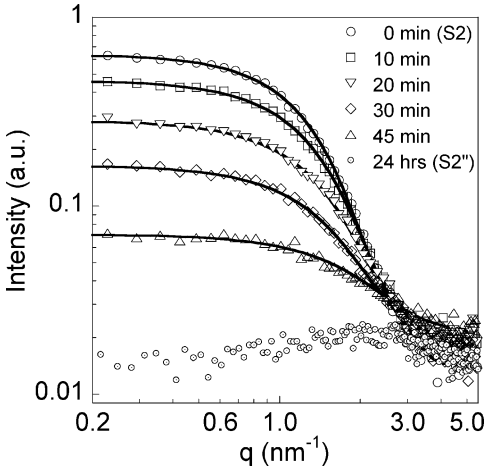

Figure 3. SAXS patterns of as-synthesized S2 sample dissolved at 25 °C. Symbols are experimental data and the solid lines are ellipsoid form factor fits (along with hard sphere structure factor) to the intensities. The final state, S2″, shows only background scattering without any detectable signal from nanoparticles in solution.

We discuss nanoparticle dissolution within the context of the aqueous silica phase diagram in Figure 2. Upon addition of silica to basic aqueous solutions, silica self-assembles at a given concentration (i.e., critical aggregation concentration), which serves as a boundary between two regions.[10,16,22] Region I is below the solubility limit of silica nanoparticles and comprises silica monomers and oligomers, whereas region II contains nanoparticles in equilibrium with soluble silica. Not shown in Figure 2 is a third region, the gelation point, which occurs at low pH (<10) and/or at higher silica concentrations (>0.7 M SiO_2).[11]

The number density of nanoparticles increases with higher concentrations of silica.[24] Particle size is a function of the solution pH,[10,11] whereby smaller particles form in more basic solutions. Nanoparticle solutions of varying composition (Table 1) were used to study the effects of size and number density on the rate of dissolution. As-synthesized nanoparticle compositions are labeled with solid symbols in Figure 2. The addition of TPAOH induces dissolution by raising the pH, while at the same time slightly lowering the total silica concentration by dilution. Figure 2 illustrates these changes for the S2 solution (dashed lines), where the open square symbol marks the solution composition at the onset of dissolution. As the nanoparticles dissolve over time, they release soluble silica. Soluble silica can undergo a series of dissociation reactions, which for monomeric species occurs by the following reaction

$$SiO_{i-1}(OH)_{5-i}^{(i-1)-} \overset{K_m^i}{\longleftrightarrow} SiO_i(OH)_{4-i}^{i-} + H^+;\ i = 1, 2, 3, 4 \qquad (1)$$

Thus, the pH decreases over the course of dissolution until the samples reach their equilibrium state, which is identified as open circles in Figure 2. The addition of TPAOH to samples S1−S6 results in the complete dissolution of nanoparticles, with the exception of solution S5.

3.1.2. Dissolution Rate, Number Density, and Size of Nanoparticles. Time-dependent changes in particle dimension were extracted from SAXS intensity curves using a form factor and a hard sphere structure factor to account for interparticle interactions. Nanoparticle shape was identified as either an oblate ellipsoid or polydisperse spheres for compositions studied in this paper.[10,11,24] Therefore, we use a uniform ellipsoid form factor to extract the radii for the *a*-axis, R_a, and *b*-axis, R_b, of the ellipsoid and report an effective sphere radius, R_{eff}, obtained from the ellipsoidal volume $R_{eff} = \sqrt[3]{R_a R_b^2}$ as a measure of the average change in particle size. Silica compositions in Table 1 were chosen for two primary reasons: (i) to maintain the dilute limit of structure factor, $S(q) = 1$, typically observed at high nanoparticle volume fractions and/or high pH,[30] and (ii) because they are representative of those used in silicalite-1 seeded growth studies[35] and Ostwald ripening experiments.[24]

Figure 3 contains representative SAXS patterns for dissolving nanoparticles. There is excellent agreement between the data (open symbols) and the form factor model (solid lines). Nanoparticle number densities were calculated from SAXS data following the procedure described by Rimer et al.[24] The number of nanoparticles remains constant throughout much of the dissolution process; however, at longer times, there is a sudden monotonic increase in the number density (see the Supporting Information). This change in number density is most likely associated with either a breakage of nanoparticles into two or more pieces or contributions to the scattering intensity from soluble silica (e.g., larger oligomers). Kinetic studies of rates of nanoparticle dissolution were conducted in the time period of constant number density. All measurements were conducted such that adequate signal-to-noise ratios are maintained over the course of dissolution. This was accomplished by selecting compositions that gave rise to large number densities, n_p, and/or particle volumes, *V*, because the scattering intensity, *I*, is directly related to these quantities by $I \propto n_p V^2$.[36,37]

(35) Nikolakis, V.; Kokkoli, E.; Tirrell, M.; Tsapatsis, M.; Vlachos, D. G. *Chem. Mater.* **2000**, *12*, 845.
(36) Lindner, P.; Zemb, T. *Neutrons, X-rays, and Light: Scattering Methods Applied to Soft Condensed Matter*; 1st ed; Elsevier: Amsterdam, 2002.
(37) Glatter, O.; Kratky, O. *Small Angle X-ray Scattering*; Academic Press: New York, 1982.

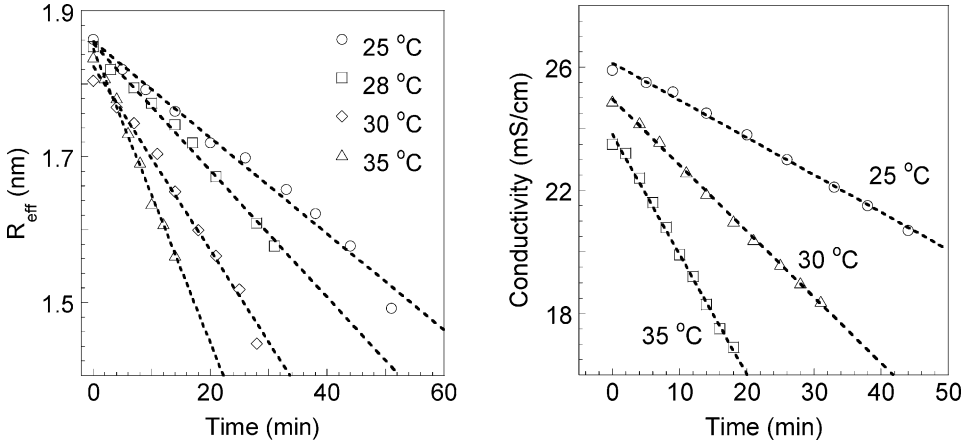

Figure 4. Dissolution of as-synthesized S4 samples at varying temperature. Plots of (a) the effective radius and (b) the ionic conductivity as a function of time. Dashed lines are linear regression of experimental data (symbols).

Table 2. Dissolution Rates of As-Synthesized Nanoparticles

			dissolution, 30 °C	
sample	(Y SiO_2)/(X OH)	$V_{t=0}$ (nm^3)	dR_{eff}/dt[a] (nm/min)	$d\sigma/dt$[b] (mS cm^{-1} min^{-1})
S1	3.0	10	−0.017[c]	−0.13[c]
S2	4.4	17	−0.010	−0.20
S3	6.7	19	−0.013	−0.22
S4	8.9	25	−0.013	−0.21
S5	8.9	25	−0.013	−0.19
S6	8.9	24	−0.012	−0.27

[a] The standard deviation of linear regression is 0.001 nm/min. [b] The standard deviation of linear regression is 0.02 mS cm^{-1} min^{-1}. [c] Rates are calculated from the linear regression of three data points

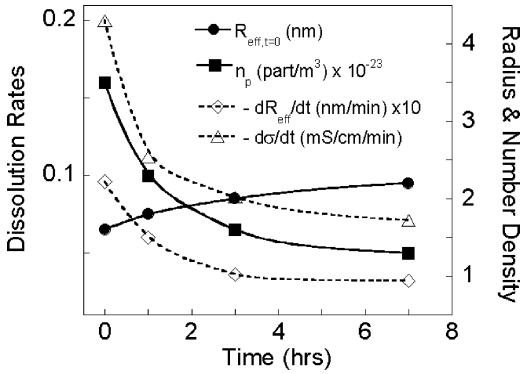

Figure 5. Right vertical axis: changes upon heat treatment of S2 samples at 70 °C over a 7 h period. During heat treatment, nanoparticles grow via Ostwald ripening, leading to a decrease in number density (squares) and an increase in the average radius (circles). Number densities were obtained from SAXS absolute intensity measurements following the procedure by Rimer et al.[24] The effective sphere radii are labeled as "$t = 0$" to indicate they serve as initial particle sizes for dissolution studies (open symbols). Left vertical axis: summary of dissolution rates vs heating time. Dissolution experiments were performed at 30 °C in 0.3 M TPAOH, resulting in decreasing rates for both dR_{eff}/dt (triangles) and $d\sigma/dt$ (diamonds).

The effective spherical radius, R_{eff}, (Figure 4a) and ellipsoidal radii, R_a and R_b (not shown), decrease linearly with time over the course of dissolution. Linear relationships between particle radius and time were also observed during dissolution of both silicalite-1 and amorphous silica (see the Supporting Information). The linear relationship indicates that nanoparticle radius, and consequently curvature, do not play a significant role in determining the rates of dissolution (see Table 2). The rates of nanoparticle dissolution, or slopes (dR_{eff}/dt) of the curves in Figure 4a, increase with temperature. From Arrhenius plots of as-synthesized particle dissolution rates over a range of temperatures (25−35 °C), an activation energy of 90 ± 8 kJ/mol (for 7 total measurements) was obtained.

The ionic conductivity, σ (mS/cm) also decreases linearly with time (Figure 4b) and follows a trend similar to that of the radius, whereby rates increase with temperature. The conductivity is predominantly controlled by the OH^- concentration because of its large ionic mobility.[24,38] The pH decreases during dissolution via the dissociation of released silica monomers (eq 1) and oligomeric species, resulting in a net reduction of solution conductivity.

Table 2 contains the measured dissolution rates of R_{eff} and σ for samples S1−S6, which are listed in order of increasing initial nanoparticle volume, $V_{t=0}$. Sample compositions span a relatively wide range of nanoparticle number density and size, which are controlled by the total silica concentration and the *Y*:*X* SiO_2:TPAOH molar ratio, respectively. We observe that the rate of nanoparticle dissolution is independent of the number density. More interestingly, the rate of dissolution shows no trend with increasing nanoparticle surface area, only small variations comparable with experimental error.

We also studied the dissolution of heat-treated particles, focusing on S2 solutions, those used in previous SAXS analyses of heat-treated nanoparticles.[24] We conducted dissolution experiments with samples pre-heated at 70 °C for various times. The right vertical axis of Figure 5 summarizes results during heat treatment. Heating results in Ostwald ripening where the number density of particles (solid squares) decreases with heating time and the average radius (solid circles) increases (i.e., the initial volume $V_{t=0}$ increases by a factor of ∼2.5 upon heating). Given the relationship $I \propto V^2$, higher particle volumes result in larger scattering intensities, helping extend the range of viable measurement. For example, SAXS studies of as-synthesized nanoparticles are limited to 10 min at 35 °C, whereas heat-treated particles can be studied over the same period at 50 °C before the particle size and scattering intensity decrease below the detection level.

(38) Castellan, G. W. *Physical Chemistry*, 3rd ed; Addison-Wesley: Reading, MA, 1983.

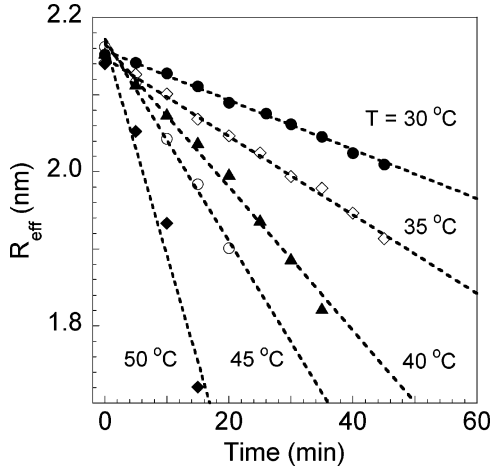

Figure 6. Changes in radius upon dissolution of heat-treated S2 solutions at various temperatures. Samples were first heated at 70 °C for 7 h prior to dissolution in 0.3 M TPAOH. Experimental R_{eff} vs time data (symbols) are shown along with linear regression (dashed lines).

Heated nanoparticles reach a relatively constant size after 7 h (solid circles in Figure 5). Dissolution of 7 h heat-treated particles at various temperatures (30−50 °C) in Figure 6 shows that the dissolution rate is temperature dependent with an activation energy of 88 ± 5 kJ/mol (5 measurements). The left vertical axis of Figure 5 summarizes results from dissolution experiments. In particular, it compares dissolution rates of nanoparticles as a function of prior heating time. Our data indicate that dR_{eff}/dt (open circles) and $d\sigma/dt$ (open diamonds) decrease the longer the nanoparticles have been heated and thus the more they have been grown. Dissolution of 7 h heat-treated nanoparticles results in a rate (dR_{eff}/dt; last open circle) that is nearly three-times lower than that of the as-synthesized nanoparticles.

3.2. Dissolution Enthalpies. Isothermal calorimetry was used to measure the enthalpies of dissolution for as-synthesized and heat-treated S2 nanoparticles and amorphous silica (Stöber particles). Given the fast dissolution rate of these silicates at room temperature, solutions were allowed to equilibrate in the calorimeter prior to TPAOH addition. The resulting heat flow curves are shown in Figure 7. Introduction of TPAOH into the nanoparticle solutions results in an initial, sharp peak followed by a second, broad exotherm that decays over time until particle dissolution is complete. As the duration of thermal treatment is increased, the secondary peaks in the heat flow curves broaden, and the time needed to reach a steady baseline increases, reflecting that lower dissolution rates lead to longer reaction times. The inset of Figure 7 illustrates the decay of the secondary peaks and the differences among heat-treated samples.

The enthalpy of silicalite-1 dissolution was measured by scanning calorimetry (see the Supporting Information), rather than isothermal calorimetry at room temperature, because of the slower rates of dissolution. Two experiments were performed with excellent reproducibility, giving an average enthalpy of −9.6 ± 0.1 kJ/mol SiO_2. Comparisons between the dissolution enthalpies, ΔH_{dis}, of nanoparticle, silicalite-1, and amorphous silica dissolution are provided in Table 3. Dissolution enthalpies of nanoparticles and amorphous silica are more exothermic than that of

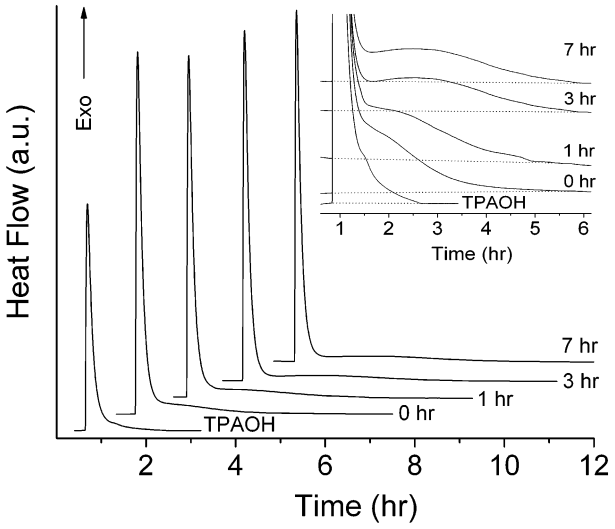

Figure 7. Heat flow curves for S2 samples heat-treated at 70 °C for various (labeled) times. Dissolution was performed in an isothermal calorimeter at 28 °C and 0.3 M TPAOH. The "TPAOH" curve was used to obtain the heat of dilution (−17.3 kJ/mol TPAOH), which was subtracted from all exothermic nanoparticle peaks to obtain the enthalpies of dissolution (see Table 3).

silicalite-1. In addition, ΔH_{dis} for nanoparticles decreases in magnitude with increased time of heat treatment.

4. Structural and Mechanistic Interpretations

Table 4 lists the activation energies of dissolution for amorphous silica, silicalite-1, and silica nanoparticles (with and without pre-heating), as well as the value for quartz reported by Dove and Rimstidt.[39] Crystalline silicates have activation energies around 90 kJ/mol, whereas amorphous silica is ∼20 kJ/mol lower. The activation energies for silica nanoparticles are independent of heat treatment and are equal in magnitude to those of the crystalline silica. This suggests that nanoparticles are more similar to the crystalline polymorphs than to amorphous silica, and therefore presumably are not amorphous, but have some degree of order. Additional, systematic differences among nanoparticles, silicalite-1, and amorphous silica are evident when comparing the rates and the enthalpies of dissolution.

Dissolution rates for various silica polymorphs are plotted in Figure 8 as a function of the initial solution pH. The disparity in experimental conditions (e.g., salt concentration and temperature) reported for amorphous silica and quartz[39] does not allow a direct comparison of rates, and thus Figure 8 illustrates qualitative trends. Two distinct features are apparent: the sigmoidal shape common to all of the curves, and the difference in magnitude of rates among silicates.

To understand the trends in dissolution rate, we draw comparisons to mechanistic studies of quartz and amorphous silica.[40−42] The rate of dissolution has taken on a general

(39) Heaney, P. J.; Prewitt, C. T.; Gibbs, G. V. *Silica: Physical Behavior, Geochemistry and Materials Applications*; Mineralogical Society of America: Washington, D.C., 1994.
(40) Rimstidt, J. D.; Barnes, H. L. *Geochim. Cosmochim. Acta* **1980**, *44*, 1683.
(41) Pelmenschikov, A.; Leszczynski, J.; Pettersson, L. G. M. *J. Phys. Chem. A* **2001**, *105*, 9528.
(42) Criscenti, L. J.; Kubicki, J. D.; Brantley, S. L. *J. Phys. Chem. A* **2006**, *110*, 198.

Table 3. Summary of Thermodynamic Data from Silica Dissolution Studies

silicate	ΔH_{dis} (kJ/molSiO$_2$)	$\Delta H_{rel\ to\ silicalite-1}$ (kJ/molSiO$_2$)	$A \times 10^3$ (m^2/mol)	ΔH_{sur} (kJ/molSiO$_2$)
nanoparticles[a]				
0 h	-23.1 ± 0.1	13.5 ± 0.1	66.3	8.6 ± 2.6
1 h	-19.2 ± 0.5	9.6 ± 0.5	58.9	7.7 ± 2.4
3 h	-18.8 ± 0.3	9.2 ± 0.3	53.0	6.9 ± 2.1
7 h	-17.8 ± 0.1	8.2 ± 0.1	48.2	6.3 ± 1.9
silicalite-1	-9.6 ± 0.1	0 ± 0.1	0	0
amorphous silica	-12.8 ± 0.2	3.2 ± 0.2	0.3	0.04 ± 0.01

[a] Times refer to the duration of the S2 sample heat treatment at 70 °C.

Table 4. Activation Energies of Silica Dissolution

silicate	E_A (kJ/mol)
amorphous silica[a]	68 ± 4
nanoparticle (as-synthesized)[b]	90 ± 8
nanoparticle (heated)[c]	88 ± 5
silicalite-1[d]	83 ± 4
quartz[e]	86

[a] See the Supporting Information. [b] S2 solution. [c] S2 solution (heat treated at 70 °C for 7 h). [d] See the Supporting Information. [e] See ref 39.

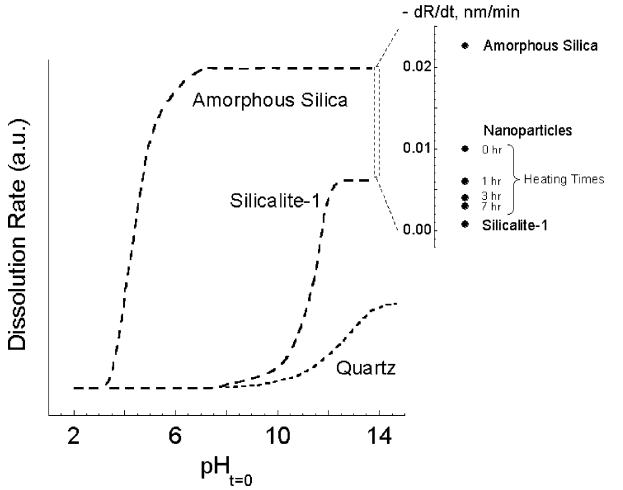

Figure 8. Dissolution rate vs initial pH for various silicates. Qualitative trends for quartz and amorphous silica were taken from Dove and Rimstidt,[39] whereas the experimental results for silicalite-1 are included in Supporting Information. The inset contains a direct comparison of dissolutions rates (nm/min) for heat-treated S2 nanoparticles, amorphous silica, and silicalite-1 at 30 °C and 0.3 M TPAOH (i.e., pH$_{t=0}$ = 13.5).

form, $r = \sum k_i C_i$, where k_i are rate constants and the concentrations, C_i, refer to surface species, ≡SiOH and ≡SiO$^-$.[43] It has been proposed that at high pH the concentration of ≡SiO$^-$ controls the rate of dissolution. Xiao and Lasaga[44] reported an *ab initio* study of a silicic acid dimer ($Si_2O_7H_6$) in which they proposed a detailed mechanism for hydrolysis of Si−O−Si bonds

$$Si_2O(OH)_6 + OH^- \rightarrow Si_2O_2(OH)_5^- + H_2O \rightarrow (Si_2O(OH)_7^-)^* \rightarrow Si(OH)_4 + Si(OH)_3O^- \quad (2)$$

The mechanism involves the dissociation of a ≡SiO−H bond, followed by the nucleophilic attack of H_2O to the Si^{+4} atom to form a fivefold coordinated silica intermediate, $(Si_2O(OH)_7^-)^*$, which subsequently leads to the breakage of the ≡Si−O−Si≡ bond. From these studies, it was concluded that the rate-determining step is the formation of the intermediate species, thus making $r = k[\equiv SiO^-]$ the rate expression for dissolution.

Trends in Figure 8 are generally consistent with this mechanism. The negatively charged surface species, ≡SiO$^-$, controls the rate of dissolution. At low pH, very few silanol groups on the silicate surface are dissociated, and low rates are observed. As the pH is raised, the concentration of negative sites increases, until very high pH is reached where the ≡SiO$^-$ concentration is nearly constant because of saturation of the surface sites. The result is the characteristic sigmoidal shape for amorphous silica, silicalite-1, and quartz, which reach steady rates around pH 7, 12, and 14, respectively.

A clear trend emerges from these studies, namely the magnitudes of dissolution rates increase in the order: quartz < TPA−silicalite-1 < amorphous silica. Dissolution rate, unlike activation energy, varies with silica structure, such that differences among crystalline materials, i.e., quartz and silicalite-1, are easily discernible. It is not clear whether one could use these differences to distinguish zeolite framework types. It is possible, though, to infer whether a material is more amorphous or more ordered from the magnitude of d*R*/d*t*.

Nanoparticle dissolution over a wide range of pH was not tested because solutions gel at lower alkalinity; however, dissolution rates above pH 11 are constant. The dissolution rate of as-synthesized nanoparticle lies between that of amorphous silica and silicalite-1 (inset of Figure 8). Thus, it is reasonable to conclude that the nanoparticles possess some degree of order, but not the crystalline framework of MFI-type zeolite. In addition, nanoparticle dissolution rate decreases with heat treatment, which according to Figure 8, suggests that heat-treated particles become more zeolite-like in structure.

Structural reorganization of silica nanoparticles during heating explains recent observations by Rimer et al.,[24] who reported that nanoparticle growth by Ostwald ripening is accompanied by a change in the composition of the nanoparticle toward that of silicalite-1 (i.e., an increase in both the neutron scattering length density and the molar ratio of TPA^+/SiO_2 in the particle core). Also, Tsapatsis and coworkers[45] reported that nanoparticles aged at room temperature for months exhibit changes in their colloidal stability (and possibly their internal structure). In particular, atomic force microscopy (AFM) measurements showed that aged particles have a greater affinity to attach to mica surfaces,

(43) Berger, G.; Cadore, E.; Schott, J.; Dove, P. M. *Geochim. Cosmochim. Acta* **1994**, *58*, 541.
(44) Xiao, Y. T.; Lasaga, A. C. *Geochim. Cosmochim. Acta* **1996**, *60*, 2283.
(45) Davis, T. M.; Drews, T. O.; Ramanan, H.; He, C.; Dong, J. S.; Schnablegger, H.; Katsoulakis, M. A.; Kokkoli, E.; McCormick, A. V.; Penn, R. L.; Tsapatsis, M. *Nat. Mater.* **2006**, *5*, 400.

an indication that changes occur within the particle, possibly because of structural reorganization and/or modifications to the surface silanol groups.

Heats of nanoparticle dissolution in Table 3 show trends similar to those of dissolution rates; the enthalpy, initially more exothermic than that of silicalite-1, changes with increased heating time to approach that of silicalite-1. Thus, thermodynamic and kinetic data both show shifts toward values characteristic of silicalite-1 over the course of Ostwald ripening.

Nanoparticle growth is accompanied by a reduction in specific surface area[24] and hence a decreased surface energy contribution to the enthalpy and free energy. Analyses of zeolites[46] have shown that with increasing particle volume, the internal surface of channels and pores becomes dominant relative to the external surface area such that zeolite enthalpies of formation are independent of the particle size. For the smaller nanoparticles studied here, the surface energy contribution is significant and determined by an enthalpic term, ΔH_{sur}, that is proportional to the surface area A as follows

$$\Delta H_{sur} = A h_{sur} \tag{3}$$

where h_{sur} is the surface enthalpy (J/m^2).

The overall energetics of nanoparticle dissolution is governed by the enthalpy term in the total free energy and the entropic contribution due to cation exchange between the particles and solution.[28] On the other hand, the stability of nanoparticles relative to a coarse solid sample is dominated by the enthalpy term in the free energy, because, as in the case of oxide nanoparticles,[47] the surface entropy term is probably small. Therefore, the thermodynamic driving force for nanoparticle dissolution can be assessed by monitoring the enthalpy of formation (ΔH_{rel}) relative to the bulk material, silicalite-1, as a function of particle size (i.e., surface area). ΔH_{rel} is calculated by taking the difference between dissolution enthalpies of a given sample and that of silicalite-1 (see Table 3). The specific surface area A (m^2/mol) is derived from the particle size using a simple geometrical model of spherical particles

$$A = \frac{3M_w}{\rho R_{eff}} \tag{4}$$

where M_w is the molecular weight (g/mol), ρ is the density (1.7 g/m^3)[24] and R_{eff} is the effective spherical particle radius (m). Using eqs 3 and 4, the surface contribution to the enthalpy relative to bulk silicalite-1 is

$$\Delta H_{sur} = \frac{3M_w}{\rho R_{eff}} h_{sur} \tag{5}$$

Comparisons of ΔH_{sur} to ΔH_{rel} in Table 3 show that surface area contributes 60−80% of the total enthalpy of nanoparticle dissolution.

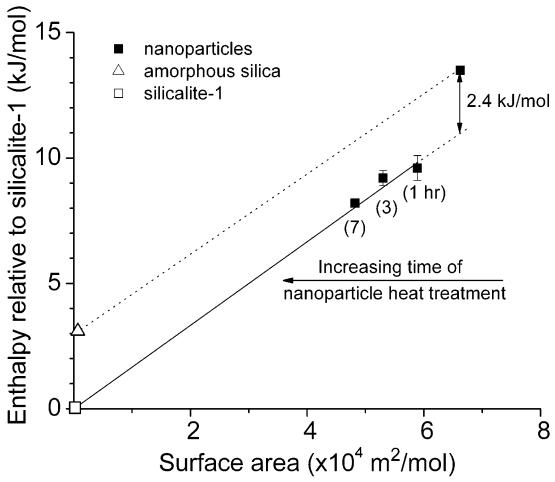

Figure 9. Dissolution enthalpies relative to silicalite-1 as a function of specific (external) surface area. The solid line is a linear fit between silicalite-1 and heat-treated S2 nanoparticles (1, 3, and 7 h) with a resulting slope of 0.17 ± 0.01 J/m^2. The dashed line is a linear fit with slope 0.16 J/m^2 connecting as-synthesized nanoparticles and amorphous silica.

Formation enthalpies are given in Table 3 and plotted in Figure 9 as a function of (external) surface area. Previous studies have shown that plots of enthalpies of formation versus surface area for mesoporous silicas and zeolites follow linear trends with slopes of 0.17 ± 0.01 J/m^2 [31,48] and 0.09 ± 0.01 J/m^2,[31] respectively. Specific surface areas of amorphous silica and silicalite-1 in this study are effectively zero given their larger particle size. Over the course of heat treatment, the total surface area of nanoparticles decreases from right to left as in Figure 9.

A line is drawn in Figure 9 between amorphous silica and as-synthesized nanoparticles, yielding a slope of 0.16 ± 0.01 J/m^2, which is similar to the surface energy of mesoporous silica. Fitting a line between silicalite-1 and the three data points of heat-treated nanoparticles gives an essentially identical slope of 0.17 ± 0.01 J/m^2, but a value that is nearly twice the surface enthalpy of zeolites obtained from Navrotsky.[31] The latter is further indication that heat-treated particles are structurally closer to amorphous silica and mesoporous phases with disordered frameworks than to crystalline zeolites.

Silica nanoparticles are metastable with respect to silicalite-1.[23] In accordance with the Ostwald step rule,[49] silica nanoparticles slowly transform into more stable structures with heat treatment, while exhibiting an exothermic enthalpy of dissolution that decreases in magnitude. This is evident both from thermodynamic (Figure 9) and structural measurements (Figure 5). From the data in Figure 9, it is clear that most changes in enthalpy occur within the first hour of heating. Subsequent heating results in similar enthalpies of dissolution (within experimental error) for the samples. This is similar to what is observed in changes in particle size. For instance, Figure 5 shows that the particles initially grow quite fast and then change very little in diameter at later times.

(46) Li, Q. H.; Yang, S. Y.; Navrotsky, A. *Microporous Mesoporous Mater.* **2003**, *65*, 137.
(47) Levchenko, A. A.; Li, G. S.; Boerio-Goates, J.; Woodfield, B. F.; Navrotsky, A. *Chem. Mater.* **2006**, *18*, 6324.
(48) Trofymluk, O.; Levchenko, A. A.; Tolbert, S. H.; Navrotsky, A. *Chem. Mater.* **2005**, *17*, 3772.
(49) Navrotsky, A. *Proc. Natl. Acad. Sci. U.S.A.* **2004**, *101*, 12096.

Dissolution studies are indirect indicators of nanoparticle structure. They do not identify changes in the local connectivity of silicon−oxygen bonds within the particle (as can be done in ^{29}Si NMR studies), nor do they identify long-range ordering of silicalite-1 framework moieties. However, dissolution offers a means of identifying trends, namely, that nanoparticles grown by Ostwald ripening exhibit increased thermal stability and modified structure toward a more connected material.

This study did not monitor the changes in water or organic content of the particles during heating. Nor did we study the distribution of water and organics in the particles, although earlier studies suggested an initial core−shell structure that evolves, with heating, into a more uniform zeolite with organic molecules in the channels.[10,12] Thus, the effects of these chemical changes on dissolution rates and on enthalpies could not be separated from the effects of changes in particle size and framework organization. Rather, the trends we see are the result of all these processes acting together. We can conclude that as the particles become more zeolite-like in enthalpy, their dissolution rates decrease. An important conclusion from our observations is that the initial nanoparticles are not simply small pieces of fully formed silicalite-1 structure but are more disordered, although distinct from amorphous silica (i.e., only partly connected with water in their silica core).

From the dissolution results presented in this paper, it is strongly suggested that nanoparticles do not possess the MFI framework of silicalite-1, and as such must undergo rearrangement upon addition to a growing zeolite surface.[50,51] Therefore, silicalite-1 crystallization occurs by one (or both) of mechanisms (1) and (2) discussed in the caption of Figure 1b, and not mechanism (3).

Results from this study also identify relevant time scales and rate-determining steps involved in the growth mechanisms listed in Figure 1b. If one is to accurately predict zeolite growth, both the forward (growth) and backward (dissolution) steps must be considered, because the overall rate of reaction is the difference of two rate processes

$$\text{Rate}_{(\text{overall})} = \text{Rate}_{(\text{growth})} - \text{Rate}_{(\text{dissolution})} \qquad (6)$$

Dissolution rates for both silicalite-1 and silica nanoparticles are presented here over a range of reaction conditions. Most striking, though, is a comparison between the rates of nanoparticle dissolution and silicalite-1 growth.[52] Kinetic studies of silica growth[26,35,53,54] give activation energies of $\sim$ 90 kJ/mol with rates (dR/dt) that are at least 15−50 times less than those of nanoparticle dissolution (depending on the degree of heat treatment). In addition, the growth rate of silicalite-1 varies between 1×10^{-3} and 1×10^{-1} nm/min depending on the pH (10−12) and temperature (60−100 °C), whereas nanoparticle dissolution is on the order 10° nm/min (at pH 12 and 80 °C). Given the mass and number densities of nanoparticles (1.7 g/cm^3, 10^{17} particles/cm^3) and silicalite-1 (2.0 g/cm^3, 10^{11} particles/cm^3),[52] there is approximately 4000 g/min of silica released during nanoparticle dissolution compared to the 30 g/min (or less) consumed during silicalite-1 seeded growth (per 1 m^3 of solution for spherical particles with radii of 1.8 and 100 nm, respectively).

Thus, nanoparticle dissolution (path M in Figure 1b) is not rate limiting in the case of a monomer addition growth mechanism. In the context of a nanoparticle addition model, our experiments do not measure the kinetics of rearrangement (i.e., path N2 in Figure 1b), but it is likely that this process is fast relative to nanoparticle addition (path N1).

5. Conclusions

We have compared the kinetics and thermodynamics of silica nanoparticle dissolution to those of crystalline silica polymorphs, such as quartz and silicalite-1, and amorphous silica. Dissolution enthalpies and rates offer an indirect method of probing the structure of silica nanoparticles, as well as their structural evolution during heat treatment. The data strongly suggest that as-synthesized nanoparticles are noncrystalline, and that over the course of heating, nanoparticles exhibit an internal reorganization toward a material that is more zeolite-like in structure, a result that qualitatively agrees with previously reported compositional changes in the nanoparticle. Data reported here are consistent with recent experiments[52] revealing the potential role of solution-mediated (i.e., monomer-based) processes in silicalite-1 crystallization, thus highlighting the importance of considering these processes as equally viable pathways in silicalite-1 syntheses. These dissolution studies identify key rates in various mechanistic steps of silicalite-1 growth that are essential for future development of predictive models of crystallization.

Acknowledgment. Dr. Andrey Levchenko is thanked for valuable discussion and comments. This work was funded by the National Science Foundation under Grant DMR 01-01391. the Nanoscale Interdisciplinary Research Team (NIRT) Grant CTS-0103010, and the American Chemical Society Petroleum Research Fund under Grant 43464-AC10.

Supporting Information Available: Dissolution of amorphous silica and silicalite-1 with radius vs time plots at varying temperature and pH along with the corresponding Arrhenius plots, SAXS analyses of as-synthesized nanoparticles with plots of number density and radii vs time, and the heat curve for the analysis of silicalite-1 dissolution by calorimetry (PDF). This material is available free of charge via the Internet at http://pubs.acs.org.

CM070708D

(50) Kirschhock, C. E. A.; Ravishankar, R.; Jacobs, P. A.; Martens, J. A. *J. Phys. Chem. B* **1999**, *103*, 11021.
(51) Kremer, S. P. B.; Kirschhock, C. E. A.; Aerts, A.; Villani, K.; Martens, J. A.; Lebedev, O. I.; Van Tendeloo, G. *Adv. Mater.* **2003**, *15*, 1705.
(52) Rimer, J. D.; Vlachos, D. G.; Lobo, R. F. Kinetics of silicalite-1 crystallization. In *Recent Advances in the Science and Technology of Zeolites and Related Materials, Parts A−C*; Proceedings of the 15th Internatioanal Zeolite Conference, Beijing, China, Aug 12−17, 2007;Elsevier: Amsterdam, 2007, in press.
(53) Twomey, T. A. M.; Mackay, M.; Kuipers, H.; Thompson, R. W. *Zeolites* **1994**, *14*, 162.
(54) Rimer, J. D.; Kragten, D. D.; Tsapatsis, M.; Lobo, R.; Vlachos, D. Growth mechanisms of silicalite-1. In *Recent Advances in the Science and Technology of Zeolites and Related Materials, Parts A−C*; Proceedings of the 14th Internatioanal Zeolite Conference, Cape Town, South Africa, Apr 25−30, 2004; Elsevier: Amsterdam, 2004; Vol. 154..
(55) Schoeman, B. J.; Sterte, J.; Otterstedt, J. E. *Zeolites* **1994**, *14*, 568.